Four-Way Microstrip-Based Power Combining for Microwave Outphasing Power Amplifiers

Citation: Barton, Taylor W., and David J. Perreault. "Four-Way Microstrip-Based Power Combining for Microwave Outphasing Power Amplifiers." IEEE Transactions on Circuits and Systems I: Regular Papers 61, no. 10 (October 2014): 2987–2998.

As Published: http://dx.doi.org/10.1109/tcsi.2014.2321203

Publisher: Institute of Electrical and Electronics Engineers (IEEE)

Persistent URL: http://hdl.handle.net/1721.1/100989

Version: Author's final manuscript: final author's manuscript post peer review, without publisher's formatting or copy editing

Four-Way Microstrip-Based Power Combining for Microwave Outphasing Power Amplifiers

Taylor W. Barton *Member, IEEE,* and David J. Perreault, *Fellow, IEEE*

***Abstract*—A lossless multi-way outphasing and power combining system for microwave power amplification is presented. The architecture addresses one of the primary drawbacks of Chireix outphasing; namely, the sub-optimal loading conditions for the branch power amplifiers. In the proposed system, four saturated power amplifiers interact through a lossless power combining network to produce nearly resistive load modulation over a 10:1 range of output powers. This work focuses on two microstrip-based power combiner implementations: a hybrid microstrip/discrete implementation using a combination of microstrip transmission line sections with discrete shunt elements, and an all-microstrip implementation incorporating open-circuited radial stubs. We demonstrate and compare these techniques in a 2.14 GHz power amplifier system. With the all-microstrip implementation, the system demonstrates a peak CW drain efficiency of 70% and drain efficiency of over 60% over a 6.5-dB outphasing output power range with a peak power of over 100 W. We demonstrate W-CDMA modulation with 55.6% average modulated efficiency at 14.1 W average output power for a 9.15-dB peak to average power ratio (PAPR) signal. The performance of this all-microstrip system is compared to that of the proposed hybrid microstrip/discrete version and a previously reported implementation in discrete lumped-element form.**

***Index Terms*—base stations, outphasing, power amplifier (PA), wideband code division multiple access (W-CDMA), Chireix, LINC, load modulation.**

I. Introduction

INCREASING demand for communications has led to complex modulation schemes intended to maximize the data rate in a restricted frequency band. The modulated signals in these systems are characterized by high peak-to-average power ratios (PAPRs), requiring the RF power amplifier (PA) to operate with linear output power control over a wide dynamic range. High PAPRs are typically associated with low average efficiencies due to the strong dependence of conventional linear power amplifier efficiency on output power amplitude. Techniques to improve efficiency over a wide output power range are therefore an important area of research and a longstanding challenge [1].

RF power amplifiers tend to achieve their highest drain efficiencies under highly saturated operation. With appropriate design, fully switched-mode operation promises the highest achievable efficiency for dc-to-rf conversion. In this limit, the transistor acts as a switch rather than a current source, minimizing intrinsic transistor loss. Although achieving true switched mode operation has historically been difficult at UHF frequencies and above due to device limitations, the development of new technologies including Gallium Nitride (GaN) high electron mobility transistors (HEMTs) has enabled drain efficiencies reaching 80% and higher at frequencies beyond 1 GHz [2]–[4]. As device performance evolves, achievable efficiency under saturated operation will continue to move closer to the limit of fully switched-mode performance.

A promising strategy to achieve high overall amplifier system efficiency with modulated signals is to employ saturated or switched-mode power amplifiers in architectures that enable overall linear response to be realized. While the Doherty architecture and its extensions (e.g., [5]–[7]) and envelope-tracking amplifier systems (e.g., [8], [9]) partially take advantage of saturated operation by utilizing saturation of the PA for a portion of the amplifier system or over a portion of the operating range, architectures that can leverage saturation (or switched-mode operation) over all or nearly all of the operating range have the potential for the highest efficiencies. Such architectures include polar amplifiers employing envelope elimination and restoration, or EER [10]–[12], amplifier systems utilizing direct load modulation of the power amplifier through electronic tuning [13]–[15], and outphasing amplifier systems [16]–[38]. Of these architectures, outphasing may represent the most readily achievable path to very high efficiency with saturated and switched-mode amplifiers.

In outphasing, power is combined from multiple "branch" PAs, with the phase-shift among the branch amplifiers used to modulate the power delivered to the load (i.e., via the vector sum of individual branch PA outputs). This technique, which was originally proposed in the 1930's [39], is able to realize high efficiency and wide-range linear output control using saturated or switched-mode power amplifiers. Outphasing may be realized with an isolating power combiner, such that the effective impedances loading the individual branch amplifiers remain constant. In this case, the PAs produce constant output power; any power not delivered to the output is delivered to another circuit port, where it is typically dissipated in an isolation resistor, though in some cases this power can be partially recovered through rectification [23]–[25]. More desirably for high efficiency under modulation, outphasing can be realized with lossless power combining [1], [16]–[20], [27]–[38]. With an appropriate lossless outphasing combiner, the PAs interact via the combiner such that variations in relative phase among the branch PAs causes the effective impedance seen by each branch PA to change, modulating the output power from each branch PA and hence modulating the total output power. (Load

The authors are with the Massachusetts Institute of Technology, Cambridge, MA, 02139 USA (e-mail: tbarton@mit.edu, djperrea@mit.edu).

This work was supported by the MIT Center for Integrated Circuits and Systems and the MIT/MTL GaN Energy Initiative.

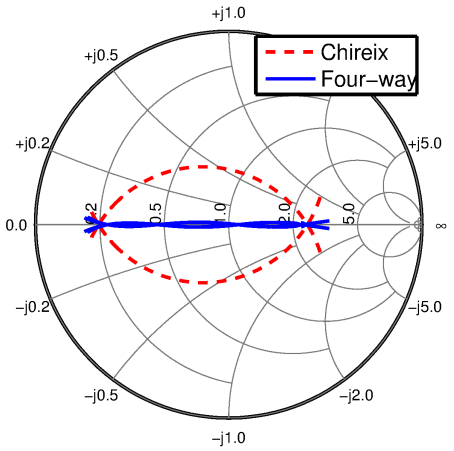

Fig. 1. A Smith chart illustrating the theoretical load impedances for the four branch amplifiers in the four-way outphasing architecture, using reactance values chosen for this work ($X_1 = 35.6\ \Omega$, $X_2 = 48.78\ \Omega$, and $R_L = 50\ \Omega$). For comparison, Chireix loading is also shown for a combiner with similar branch amplifier operating conditions.

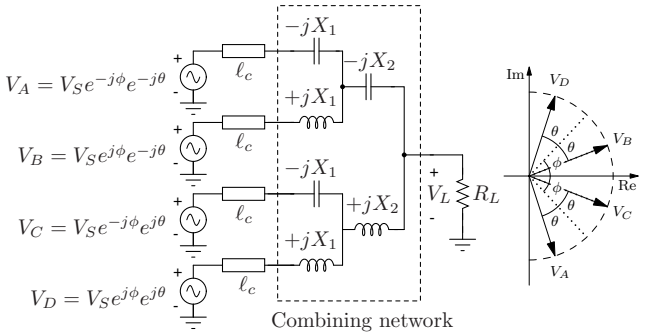

Fig. 2. Lumped element implementation of the four-way outphasing and power combining system. The PAs are represented as ideal, constant-amplitude voltage sources with the phasor relationship shown. The interconnects from the PA reference planes to the combiner input reference planes are represented as transmission line segments [16].

modulation under outphasing is similar in some regards to the load modulation effect in Doherty amplifiers, albeit realized through phase-shift control of saturated branch PAs rather than RF drive amplitude control.) For appropriately-designed branch PAs (e.g., [6], [37], [38], [40], [41]), high branch PA efficiency can be maintained across a wide range of resistive load impedances, yielding high overall efficiency under modulated conditions. Outphasing with lossless combining using switched-mode branch PAs may have the potential for the highest overall efficiency in modulated power amplifier systems.

A significant limitation in traditional approaches to outphasing with lossless combining is variable reactive loading of the branch power amplifiers across the outphasing range. Power control is achieved through the modulation of the real component of the effective loading impedance/admittance seen by the branch PAs. Unfortunately, most lossless outphasing systems — including the traditional Chireix combiner — also yield substantial reactive/susceptive variations in the effective loading of the branch amplifiers. This variable reactive loading tends to hurt efficiency, both due to the added conduction losses associated with the reactive currents and because many high-efficiency PAs (including switched-mode RF amplifiers) are sensitive to load impedance, and branch PA efficiency can degrade under (variable) reactive loading.

The outphasing system presented in this work provides nearly ideal resistive load modulation to the branch PAs. Used in conjunction with saturated and switched-mode PAs suitable for load modulation operation (e.g. [6], [40]), high efficiencies can be achieved. In principle, it is possible to approach the ideal efficiency of a fully lossless, switched-mode system with this approach. In the outphasing approach explored here, four PAs are power combined and outphased. As compared to a traditional Chireix in which two PAs are outphased, use of four branch PAs with an appropriate combiner and control enables much more nearly resistive loading of the branch power amplifiers to be achieved, as illustrated in Fig. 1 [28].

The initial demonstrations of this four-way outphasing and combining architecture used a version of the combining network incorporating lumped elements in a tree structure as shown in Fig. 2 [16], [42]. While this combiner is quite compact and effective, at microwave carrier frequencies there are practical issues with this implementation relating to the non-idealities of the discrete elements and their interconnections, particularly as regards series connections in the power path. First, repeatable tuning of the components for high performance at microwave frequencies is challenging: undesired parasitic shunt capacitance to substrate at intermediate nodes can affect the performance of this combiner network. It can also be challenging to manage the effect of phase shifts through the network due to nonzero component electrical lengths. Moreover, component losses (especially dielectric loss of capacitors in the series path) can present limits to achievable power rating at microwave frequencies. Improved means of realizing lossless multi-way outphasing are therefore desirable.

In this work, we present and compare two implementations of multi-way lossless power combiners for outphasing that incorporate microstrip transmission lines. We present a hybrid microstrip/lumped element implementation that retains the tunability of a discrete-element design while limiting the use of lumped elements to ground-referenced shunt connections where non-idealities are more readily absorbed.[1] This technique can also be applied with non-microstrip transmission-line structures. We also introduce a new all-microstrip design incorporating microstrip transmission lines and radial stubs. This approach is also demonstrated experimentally, and its several advantages including greater manufacturability and power handling capability are discussed.

Section II of the paper presents the development of the new four-way power combining networks, along with implementation details and simulations of both networks over a range of carrier frequencies. Section III presents the mixed mode signal decomposition used in the prototype system, which is based on

[1] A preliminary demonstration of this idea appeared in the authors' conference paper [43], and is demonstrated here at higher performance levels with a re-tuned combining structure.

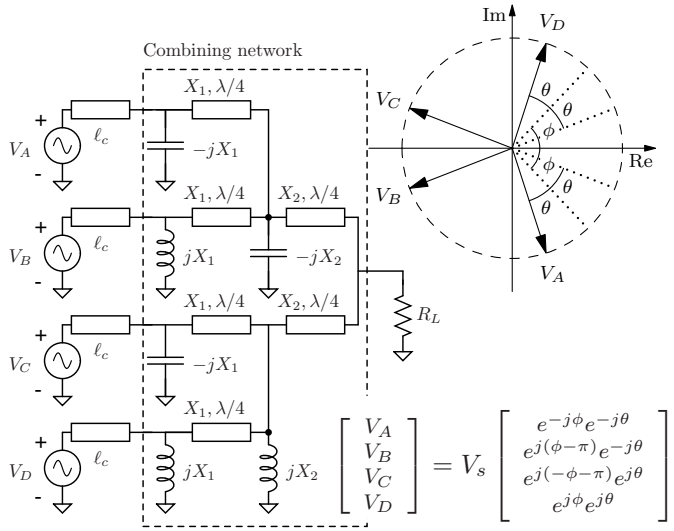

Fig. 3. Four-way power combiner implementation using shunt reactive components and transmission-line sections, and phasor relationship of the four PA input voltages. The PAs are represented as ideal voltage sources [43].

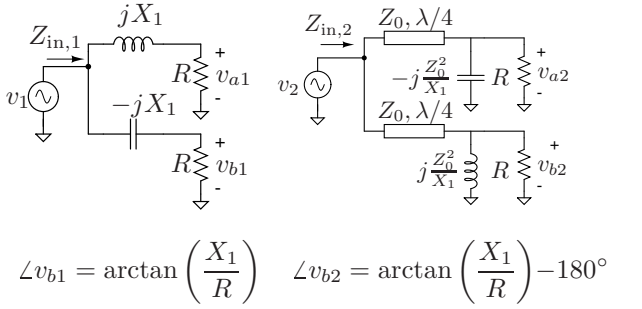

Fig. 4. Network transformation between two variations of the single-stage resistance compression network [43]. Input impedances and terminal voltage amplitudes are identical.

a combination of a theoretical control law and experimentally determined input power conditions. The remaining system components, including the branch amplifiers, interconnects, and baseband signal processing are described in Section IV. In Section V, measurements of each combiner in an outphasing power amplifier system are presented and compared. A Chireix outphasing system is also implemented and measured for a direct comparison of the techniques. Finally, Section VI concludes the paper.

II. Power Combining Network

A. Theoretical Development

In this work, we present two combining networks related to the all-discrete one in [16] (see Fig. 2) but which incorporate transmission lines to overcome some of its limitations. Although the discrete-component implementation has been successfully demonstrated for microwave power amplification, realizing the design relies on extensive hand-tuning of component values. Furthermore, the connection of discrete elements in series in the power path introduces both power handling limitations and non-negligible electrical length which interferes with the outphasing operation by introducing undesirable phase shift. At GHz and higher frequencies, it is preferable to utilize transmission lines in the power path and limit the use of discrete elements to ground-referenced shunt connections, as in the new network topology in Fig. 3. In this configuration, the parasitics and electrical lengths of the lumped elements can be more readily absorbed into the component values.

TABLE I
Measured and ideal S_{21} port relationships for the combiner implementations studied in this work.

	Radial Stub		Hybrid μ-strip/ Discrete		Ideal
Port	Ampl.	Phase	Ampl.	Phase	Phase
A	0.95	88	1.01	86	88
B	0.96	-163	0.98	-164	-163
C	1.04	162	1.02	165	163
D	1.06	-88	0.98	-85	-88

Note: amplitude measurements have been normalized to 1 to facilitate balance mismatch comparison. Given this normalization, the ideal amplitudes for each port is 1.

The microstrip-based combining network in Fig. 3 is related to that in Fig. 2 through the network transformation shown in Fig. 4 [43]. The two networks shown have nearly identical port relationships, with $Z_{\text{in},1} = Z_{\text{in},2}$, $|v_{a1}| = |v_{b1}| = |v_{a2}| = |v_{b2}|$, and $\angle v_{a1} = \angle v_{a2}$, but with phases $\angle v_{b1}$ and $\angle v_{b2}$ differing by 180° as indicated in the figure. Applying this transformation and keeping track of this phase difference in the control law definition (see Figs. 2 and 3), the two combining networks will have identical effective input impedances at the corresponding input ports when the input voltages have the indicated relationships. (By "effective" input impedance, we mean the complex voltage-to-current ratio at a port with the other ports driven as indicated.) These input impedances are nearly resistive when the input phases are described by the outphasing control law in (1), which relates control angles ϕ and θ to commanded output power P_N:

$$\theta = \cos^{-1}\left(\sqrt{\frac{P_n}{4} + \frac{1}{4P_n}\left(\frac{X_1}{R_L}\right)^2}\right), \qquad \phi = \tan^{-1}\left(\frac{X_1}{R_L P_n}\right) \tag{1}$$

The net phase of the output signal can be controlled by adding an offset phase to all four branch PA signals. These equations have been normalized such that for $P_N = 1$ the real part of the load impedance seen by each branch amplifier is equal to 50 Ω. This control law minimizes the susceptive components of the branch amplifier load impedances [32].

For the combiner component values used in this work, $X_1 = 35.6\ \Omega$, $X_2 = 48.78\ \Omega$, and $R_L = 50\ \Omega$, the phase of the load admittance seen by each branch amplifier is calculated to be ideally under 2° over a 10-dB range of output power [32]. Fig. 1 shows the resulting branch amplifier loading conditions for either of the combining networks in Figs. 2 and 3. It is clear from this figure, which also includes load impedances for a Chireix combining network operating over a similar impedance range, that the four-way combining network offers considerably improved branch amplifier loading conditions.

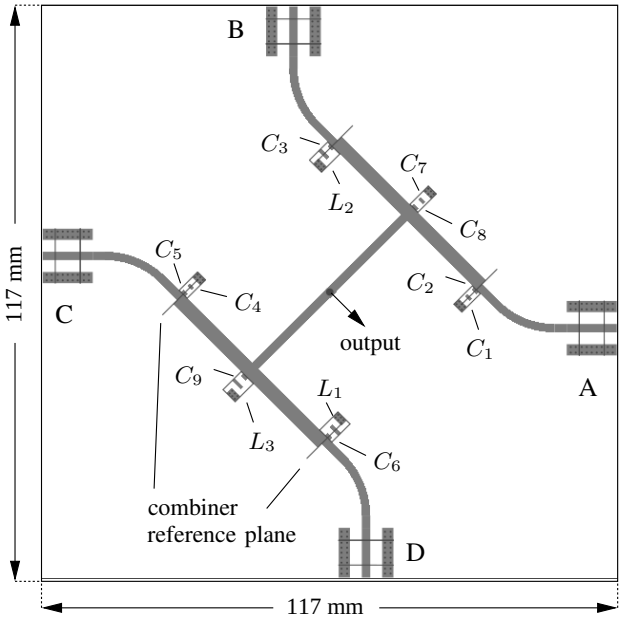

Fig. 5. Top copper layout of the fabricated hybrid microstrip/discrete combiner. Input reference planes are indicated in silkscreen. Each shunt reactance is implemented with two series components (L-C or C-C) to facilitate tuning.

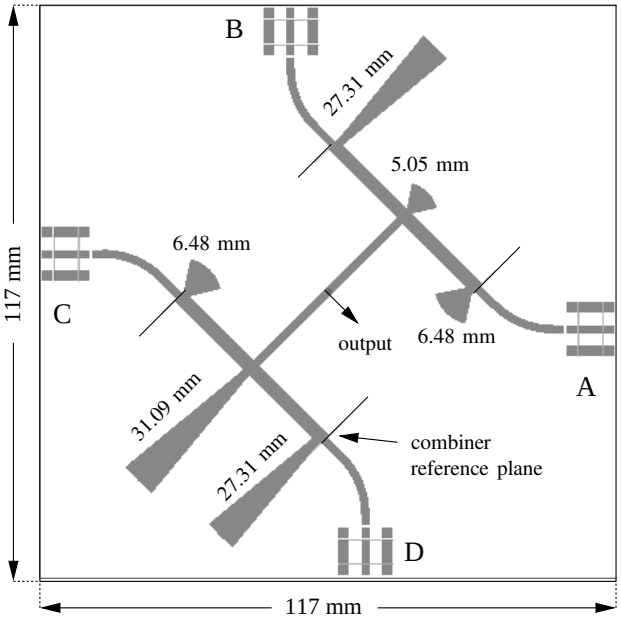

Fig. 6. Top copper layer of the fabricated radial stub combiner, with radial stub lengths indicated. The bottom layer is a ground plane, with the exception of a vertical SMA connector at the center output connector on the underside of the board.

B. Hybrid Microstrip/Discrete Combiner Implementation

The network in Fig. 3 can be directly implemented by using microstrip transmission lines with discrete components to realize the shunt reactive elements [43]. The hybrid microstrip/discrete combiner readily absorbs discrete component nonidealities (shunt capacitance, non-zero electrical length) by only using them in shunt connections to ground. At the same time, it still requires a significant component tuning effort in order to produce the desired amplitude and phase relationships between the ports. The layout of the fabricated 0.762-mm thick Rogers RO4350 combiner PCB is shown in Fig. 5. The fabricated structure uses series-connected $L-C$ and $C-C$ combinations to allow for tuning, particularly of the inductive branches due to the widely-spaced component values available. The output power is taken from a modified vertical SMA connector on the underside of the board. The ground pins of a through-hole connector are ground down to the length of a surface mount vertical SMA connector, and the center pin is cut down to be flush with the top of the combiner board when inserted through the center hole. Other than the footprint for this connector, the bottom plane of the board is a continuous ground plane.

Component values are selected through an iterative trimming process to absorb the nonidealities of the components. In this process, the network is driven in reverse (i.e. as a power splitter) and the phase and magnitude of the forward voltage gains to the four 50-Ω-terminated ports are compared to the theoretical values. The component tuning process is described in detail in the appendix. For this work, the combiner was carefully re-tuned for a closer match between theoretical and measured port relationships (see Table I); component values are given in Table II.

TABLE II
TABLE OF COMPONENT VALUES

Component	Value	Mfr. Part #	Mfr.
C_8	1.1 pF	600F 1R1BT	American
C_3, C_6, C_9	1.5 pF	600F 1R5BT	Technical
C_7	2.0 pF	600F 2R0TC	Ceramics
C_1, C_4,	2.4 pF	600F 2R4BT	Corp.
C_2, C_5	2.7 pF	600F 2R7BT	
L_1-L_3	3.85 nH	0906-4GLB	CoilCraft

C. Radial Stub Combiner Implementation

The hybrid microstrip/discrete implementation has several advantages over the series-component combiner in Fig. 2, but still requires significant hand-tuning of component values in order to synthesize the network. It is desirable to implement the combining network using only microstrip elements to gain the benefits of this power combining approach in a way that is easily repeatable and does not require precision component mounting. The network in Fig. 3 is an ideal basis for an all-microstrip implementation as it already includes transmission line components and the shunt reactive elements can be realized with microstrip structures. We implement the transmission lines in microstrip and the $\pm jX_1$ and $\pm jX_2$ reactive elements using open-circuit radial stubs.

According to simulation, the reactance of the chosen stubs varies by only $\pm 5.2\%$ over the frequency range 2110-2170 MHz in the worst case ($+jX_2$). For comparison, the simulated reactance of an open-circuited, uniform-width 50-Ω stub synthesizing the same reactance varies by $\pm 6.8\%$ over that range. Discrete-element shunt reactances have the lowest frequency variation even considering the use of discrete LC-networks to

realize the reactances needed (in order to overcome limitations in available discrete inductor values). For example, variation of the $+jX_2$ shunt reactance with ideal components in the hybrid microstrip/discrete implementation is only $\pm 1.6\%$ over the same frequency range. Consequently, the hybrid microstrip/discrete and radial stub implementations exhibit a trade-off in which ease of fabrication can be exchanged for combiner bandwidth. Note that the radial stub combiner also has advantages in scalability to higher operating frequencies and, as will be seen in Section V, in improved power handling capability.

The layout of the combiner implementation is shown in Fig. 6. Stub lengths are designed based on theoretical values, then adjusted in simulation with Agilent ADS. The angle subtended by the capacitive stubs is 65° while the inductive stubs subtend 11° [44]. These values were chosen to be as large as practical while limiting unwanted coupling. Similarly, the orientations of the radial stubs with respect to the combiner structure were chosen to reduce coupling. The output port on the underside of the PCB is fabricated in the same way as for the hybrid microstrip/discrete combiner.

Each combining network was fabricated on a 0.762-mm thick Rogers RO4350 substrate and characterized as in [16], [43] by driving the output with a vector network analyzer and measuring the amplitude and phase relationship at the four inputs when all ports are terminated in 50 Ω. That is, the networks are characterized by observing their action as a resistance compression network [28], [45] loaded at 50 Ω. This enables convenient measurement of the characteristics expected under power combining conditions. The measured S_{21} results in Table I indicate excellent matching, with the radial stub combiner having phases within one degree of ideal, along with amplitude variation with worst case error of 6%. Similarly, the hybrid microstrip/discrete combiner, re-tuned from [43] for this work, has phase matching within 3 degrees of ideal and amplitude variation within $\pm 2\%$. Amplitudes have been normalized to emphasize the minor balance mismatch between the four ports.

D. Combiner Bandwidths

The RF bandwidth of each combiner can be characterized by an ac sweep of the transmission coefficient of a back-to-back pair of networks, with one network in each pair acting as a splitter. The simulation results for ideal networks of the three implementation types (series discrete, hybrid microstrip/discrete, microstrip with radial stubs) are shown in Fig. 7, with -0.5 dB bandwidths indicated. The two transmission-line-based combining networks have under half of the operating bandwidth of the ideal discrete power combining network in this simulation, with the radial stub combiner the most narrow-band of the three. Nevertheless, all three show bandwidth sufficient for many practical applications.

A further consideration relating to combiner operating bandwidth is the effect on the load impedances seen by the four branch amplifiers at different operating frequencies [46]. Fig. 8 shows the power factor associated with the effective load impedances seen by the branch amplifiers across power for

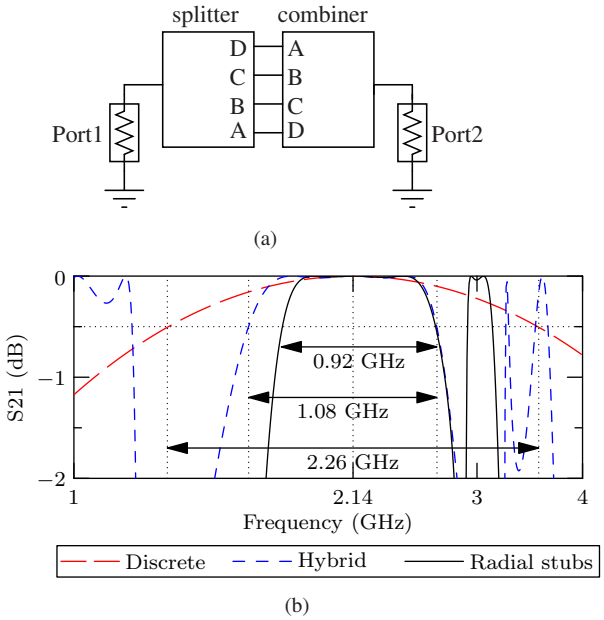

Fig. 7. Simulation computation of combiner bandwidths in back-to-back connection. (a) - simulation configuration; (b) - ac sweep results.

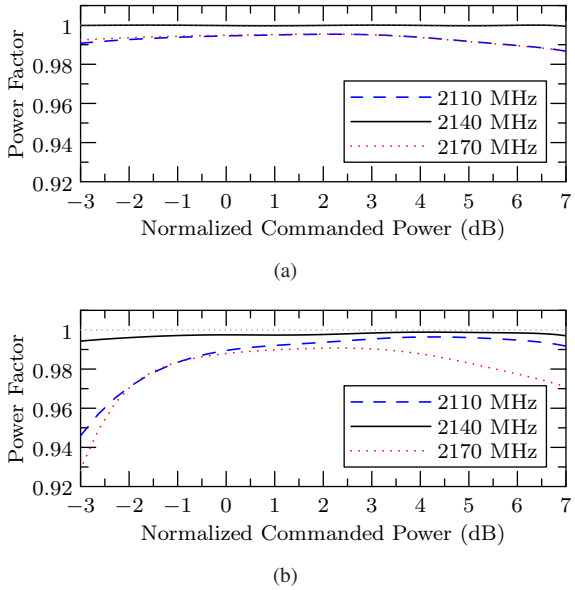

Fig. 8. Simulated average power factor seen by the branch amplifiers for a given commanded power at 2110 MHz and 2170 MHz, (a) - hybrid microstrip/discrete combiner, (b) - radial stub combiner.

three different operating frequencies. The power factor directly reflects the degree of reactive loading seen by the branch amplifiers. The simulation results in Fig. 8 are based on the Agilent ADS model of the two fabricated combining networks. As shown, in each case the average power factor of the four loads is somewhat lower at the extremes of the 60-MHz range. For a power amplifier in which drain efficiency is proportional to power factor, a corresponding drop in drain efficiency would be expected. The hybrid microstrip/discrete implementation has higher overall power factor because of its wider operating bandwidth.

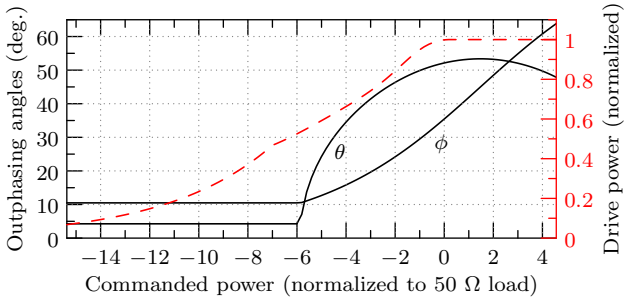

Fig. 9. Signal decomposition in the four-way outphasing system, shown for the radial stub combining network. The outphasing angles follow the theoretical control law in (1).

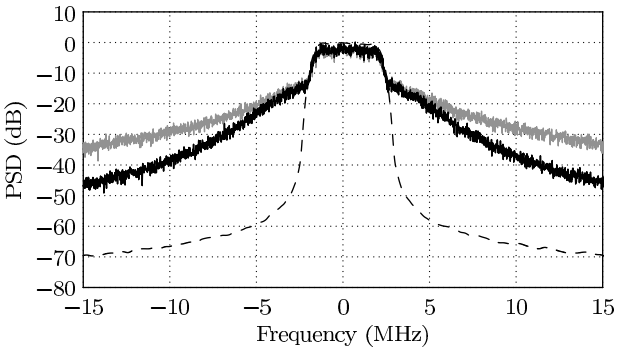

Fig. 10. Bandwidth expansion due to outphasing signal decomposition. The plot shows the original W-CDMA spectrum (dashed lines), spectrum of Chireix outphasing branch signals (grey), and spectrum of 4-way outphasing branch signals (black). The 4-way system simulated to generate this plot uses outphasing for the upper 7.5-dB of the power range, then drive amplitude modulation for lower output powers.

III. Input Signal Decomposition

In classical outphasing, the branch amplifiers are considered to be driven by constant-amplitude inputs of sufficient amplitude to drive them into saturation. In practice, however, input power modulation (RF drive modulation of the branch amplifiers) is included. Given the finite operating range where load modulation is predominantly resistive (here, the upper 10-dB), it is advantageous to use RF drive modulation below this range to extend to lower output powers. This capability is particularly important for modulated signals with zero crossings. Furthermore, reducing the input drive amplitude while outphasing for lower output power levels improves the power-added efficiency (PAE) of the system and avoids over-driving the branch amplifiers. The four-way outphasing system therefore has three regions of operation: pure outphasing with constant (maximum) drive amplitude; mixed-mode operation where drive amplitude is used to avoid over-driving the branch amplifiers, but the primary output power control mechanism is outphasing; and drive modulation only, where the input power does not drive the branch PAs into saturation. In the first two regions, the branch PAs are driven with sufficient input power to operate in a saturated mode, with the drive amplitude reduced as the input power required for saturation decreases with system output power. In the mixed-mode region, the amplitude drive control law uses a rational equation fit to experimentally-determined points where the branch amplifiers are saturated but not over-driven. These values are determined for each combining network by sweeping the input power for various constant outphasing angles and observing the saturation behavior. The signal decomposition for the radial stub combiner is shown in Fig. 9. The phase signal decomposition is performed in both the pure outphasing and mixed-mode regions following the theoretical outphasing control laws in (1). In the lowest-power mode where outphasing angles are held constant and drive amplitude modulation is used, the branch PAs no longer operate in efficient saturated mode. This drive-amplitude-only control region occurs at powers below a 10-dB backoff from peak output power.

A. Bandwidth Expansion

In addition to the RF bandwidth of the combining network, another bandwidth consideration relates to the nonlinear transformation between the desired transmit signal and the individual branch signals. The resulting bandwidth expansion is a common feature of outphasing amplifiers, and can limit the achievable transmitted signal bandwidth. In Fig. 10, the spectrum of the branch signals in the four-way outphasing system is compared to that of the ideal W-CDMA spectrum (dashed lines). This plot is based on the signal decomposition described above, in which outphasing is used for the upper power range, and drive amplitude modulation is used for low output powers. The spectrum of Chireix outphasing branch signals is also shown. Because the bandwidth expansion of the four-way outphasing system is similar to, but slightly less than, that of Chireix outphasing, it is expected that the four-way system does not pose additional bandwidth (and hence linearization) challenges beyond those of Chireix systems.

IV. System Implementation

The two four-way combining networks are directly compared by characterizing them both in the same system; i.e. using the same RF power stage and baseband signal generation. These system elements are described in this section. Note that although the basic components of this experimental system are similar to those in [16], for this work the power amplifiers were re-tuned for higher efficiency and a modulated test signal with higher PAPR was used.

A. Inverse Class F Power Amplifier

The prototype outphasing system RF power stage, shown in Fig. 11, includes four inverse class-F PAs using the design in [6]. These are the same branch amplifiers used in [16], [43] but with some adjustment of components to improve drain efficiency. The output power and drain efficiency of all four branch amplifiers operating with at 28 V supply have been characterized using a stub tuner loading each branch PA over a range of real load impedances similar to those that they see in the combiner system. The measurements of the individual branch PAs are shown in Fig. 12(a). To understand the potential performance of these branch PAs in an outphasing system, the branch PA output powers are summed assuming

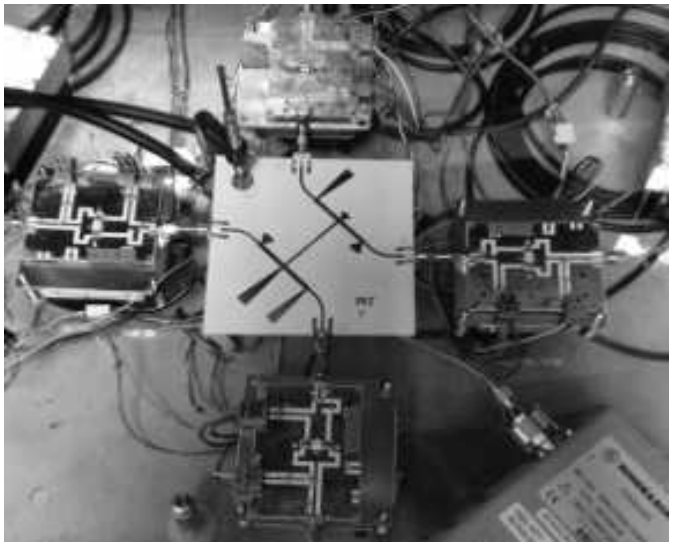

Fig. 11. Photograph of the RF power stage of the outphasing system. The final-stage branch PAs and the radial stub microstrip combiner are shown.

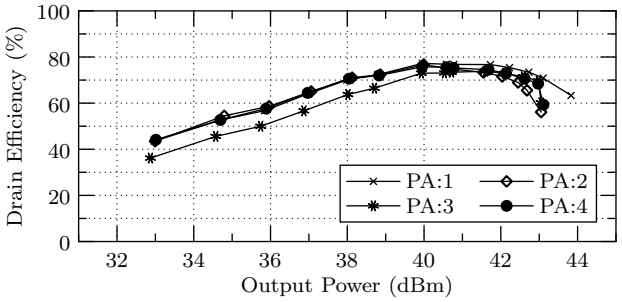

(a)

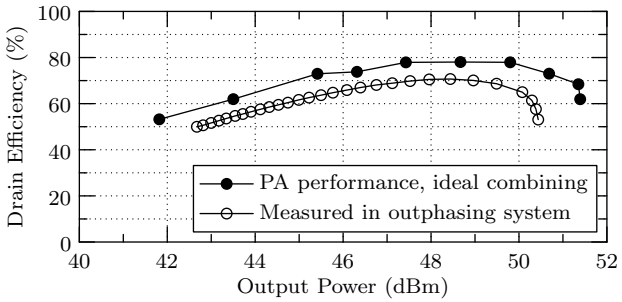

(b)

Fig. 12. Measured drain efficiency and output power for constant drive amplitude: (filled) - calculated from individual characterization of the branch amplifiers and assuming zero-loss power combining; (open) - experimentally measured system performance using outphasing control.

ideal power combining (zero loss), and drain efficiencies are averaged. For these measurements a constant drive amplitude is used that is sufficient to saturate the branch amplifiers at the highest output power. The resulting curve shown in Fig. 12(b) represents the highest achievable performance of any power combining system using these branch amplifiers and drive conditions. Although some mismatch can be seen between the four PAs, the measured outphasing system (also shown) closely matches the expected performance. As can be seen in Fig. 12, the branch PA efficiency drops sharply at high power levels; this characteristic curve shape also appears in the outphasing system measurements. In practice, the efficiency will be degraded due to combiner insertion losses as well as any non-idealities in loading conditions.

By comparing the shape of the two curves in Fig. 12, it can be seen that the insertion loss of the combiner is consistent across power level. In particular, the similarity in form between the two curves indicates that the branch amplifier loading conditions are close to the resistive loading conditions under which the branch amplifier characterization was performed. Likewise, it is demonstrated that the combiner operates at reasonably high efficiency ($\sim 90\%$ or ~ 0.45 dB insertion loss), though not perfectly losslessly due to practical considerations.

In addition to drain efficiency, system PAE is an important metric for the system performance. However, in situ measurements of overall PAE is made difficult by the system complexity. In order to provide an estimate of system PAE, therefore, a single branch PA was characterized with both load and input drive modulation. In an analogous manner to the signal decomposition as described in Section III, the PA is loaded with various resistance values, and for values greater than 50 Ω (corresponding to $P_N < 1$, following the control law indicated in Fig. 9) the drive magnitude is chosen to saturate but not overdrive the amplifier. The resulting relationship, shown in Fig. 13, highlights an advantage of this resistive load-modulation-based topology; namely, that both a high gain and a high efficiency can be maintained in the branch PAs over a wide range of output powers, so that high PAE is maintained along with drain efficiency. This measurement illustrates gain and PAE of the constituent branch amplifiers under load modulation, and will be used to estimate the overall system PAE in Section V.

B. Connectors Between PAs and Combiner

In load modulation based systems, the electrical length of the interconnect between the combiner input reference plane (see Fig. 6) and the reference plane of the drain of the device is critical. This length must be an integer number of quarter-wavelengths for the resistive loading to be maintained. In this prototype, where a connectorized design is used in order to facilitate testing and comparison of different combiner implementations, the net path between these reference planes includes the branch PA PCB and combiner PCB traces as well as the SMA interconnects. In the prototype system, it was found that including a male-to-female SMA adapter in each branch between the combiners and PA provided a net quarter-wave electrical length at 2.14 GHz. This arrangement is indicated for a single PA input path in Fig. 14. With each of these SMA adapters alone contributing 0.045 dB to the insertion loss of the combiners, it is clear that a non-connectorized design would give improved efficiency performance.

In order to compensate for the impedance inversion resulting from the net quarter-wave connection between the reference planes of the combiner and active device, the control law in (1) is modified by replacing P_n with $1/P_n$ in the signal separation

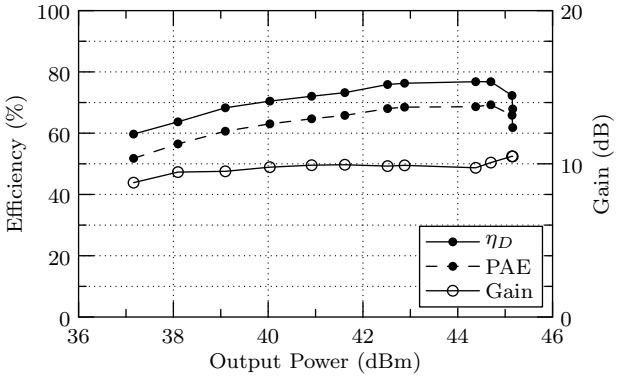

Fig. 13. Performance of a single branch PA under load modulation when the input drive magnitude is adjusted to saturate but not over-drive the amplifier. The drive levels are analogous to those used in the outphasing system (outphasing plus drive backoff). The gain, which is flat over the range of power levels considered, is used to estimate system PAE.

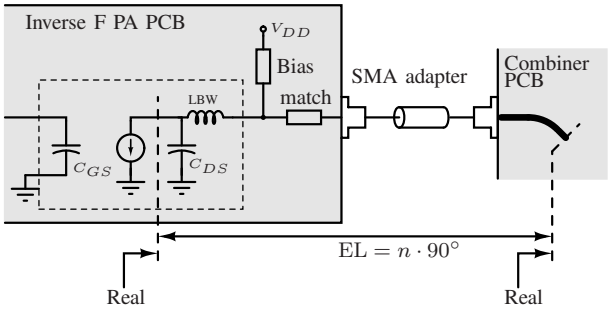

Fig. 14. A partial sketch of the connectorized RF power stage. The interconnect length between the reference planes of the combiner input and the drain of the device is critical; it must be chosen as an integer number of quarter wavelengths to provide resistive loading to the device.

computation [16]. For clarity, we omit this inversion in the discussion of signal separation in this paper.

C. DPD Implementation and Limitations

The dynamic performance of the outphasing system is characterized using a W-CDMA signal with 3.84 MHz bandwidth generated using Agilent ADS. The signal is hard-clipped to reduce its PAPR to 9.15 dB, at the cost of achievable ACLR. The signal processing chain utilized in the prototype system, while sufficient for demonstrating the system performance and efficiency, limited the degree to which digital predistortion for high linearity could be realized. The signal processing approach and system components are described as follows.

IQ modulators are implemented using Analog Devices AD9779A DAC evaluation boards, driven by a Virtex-5 FPGA. The baseband data is clocked at 30.72 MSPS, and the maximum test signal length is 8192 points due to memory limitations in the FPGA. A combination of effects including this short signal length and hardware limitations constrains the ACLR that the baseband generator can produce. With this configuration, a single IQ modulator transmitting the test signal has an ACLR_1 of only -37.7 dBc. As a result, the achievable ACLR with this prototype is severely limited.

The receiver side is similarly limited, with an 8-bit, 20 GSPS oscilloscope used along with Agilent VSA software to perform direct downconversion on the 2.14-GHz modulated RF signal. The downconverted signal is manually time-aligned and compared to the transmitted signal in MATLAB. Based on a comparison between the nominal and received signals, memoryless LUTs correcting amplitude and phase are updated in MATLAB.

It is important to note that all four PAs are driven into saturation during outphasing operation. As can be seen in Fig. 12, the branch PAs have some mismatch in saturation power. For this demonstration, we ignore the mismatch rather than attempting to create equal output powers by either: (a) reducing the drive on the strongest three branch amplifiers to match the lowest output power, therefore operating them in a nearly-saturated Class B mode, or (b) trimming either the gate bias voltage or introducing other intentional mismatch in the branch amplifier construction, and potentially introducing other undesirable asymmetry in the system. When the system is operated in mixed-mode or amplitude-only control, on the other hand, a set of static LUTs is used to relate the output powers and phases of each branch amplifiers to the desired value. These LUTs compensate for the different branch amplifier behaviors under drive backoff, particularly AM/PM distortion which would potentially cause loading mismatch in the outphasing system. The memoryless LUTs performing this predistortion are populated by measuring the output amplitude and phase of each branch amplifier into a 50-Ω load in CW.

As a result of the limited DPD implementation, this work does not address linearization of the architecture in depth. Because the four-way outphasing amplifier has nonlinearities and structure similar to those of Chireix amplifiers, it is reasonable to expect that similar linearities are achievable with the two amplifier architectures. Furthermore, an advantage of the four-way system is that the four branch PAs see very similar load impedances, as compared to Chireix in which one branch is loaded capacitively and the other inductively. These loading conditions can help the linearity of the amplifier system, in that if the individual branch amplifiers are prone to AM/AM and AM/PM distortion, the close match between loading conditions means that their behavior will vary together. Referring to the ACLRs achieved by [37], [38], [47] as shown in Table III, we therefore expect that it will be possible to meet the W-CDMA mask requirement using memoryless DPD.

V. Measured Performance

A. 4-Way System CW Outphasing Measurements

Outphasing performance is characterized for each combiner implementation by varying the relative phase and amplitudes of the four CW branch PA inputs following the control law described in Section IV. The hybrid microstrip/discrete network was found to have power limitations in tests above 60 W peak power due to the lumped reactive elements. Therefore, for a direct comparison between these networks, we characterize both combiners at a lower power level (20-V branch amplifier power supplies) as shown in Fig. 15. The drain efficiency of the hybrid microstrip/discrete combiner remains over 50%

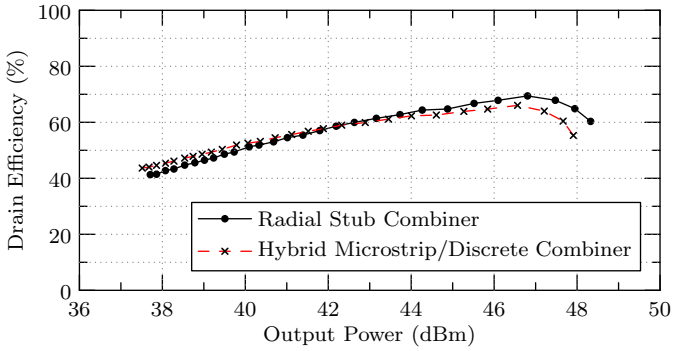

Fig. 15. Low-power (20-V drain bias supply) CW outphasing measurements comparing the radial stub and hybrid microstrip/discrete combiners at 2.14 GHz.

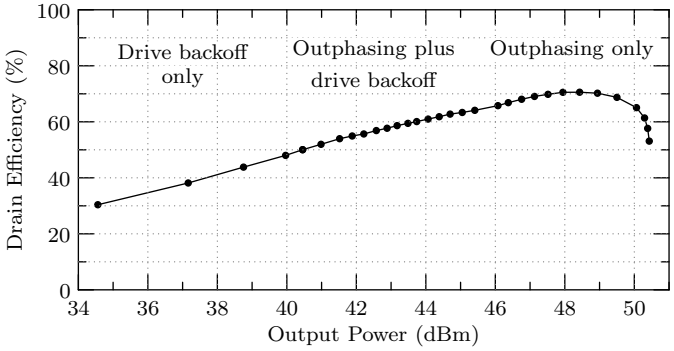

Fig. 16. CW outphasing measurements of the power amplifier system at a 2.14-GHz carrier and using the radial stub combining network (with 28-V drain bias supply), with the signal decomposition shown in Fig. 9.

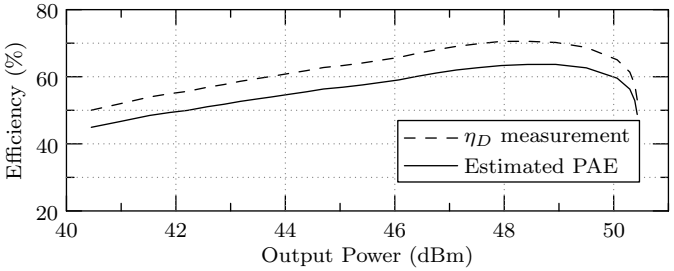

Fig. 17. Estimated radial combiner system PAE, based on the measured outphasing system drain efficiency (Fig. 16) and the gain of a single branch PA characterized under resistive load modulation (Fig. 13).

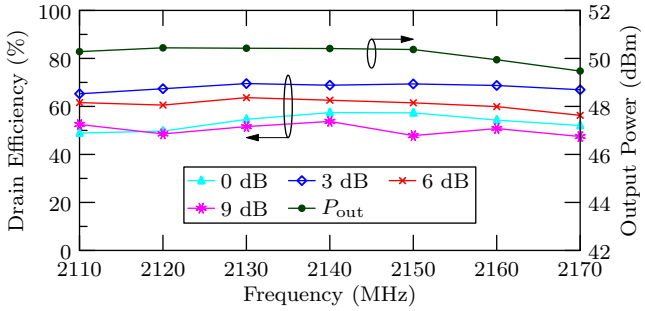

Fig. 18. Peak output power and drain efficiency, measured at different power back-off levels, shown as a function of frequency over the 2110–2170 MHz range required for W-CDMA.

over an 8.4-dB power range, and above 60% over the upper 4.8 dB of the range. This performance is an improvement over that of the all-discrete-element combiner, for which the non-ideal behavior of the combiner introduced compression in the outphasing/output power relationship such that the drain efficiency is over 50% for only a 7-dB range [16].

The results in Fig. 15 indicate that the performance of the two combining networks are similar at low power levels, but that the efficiency of the hybrid microstrip/discrete combiner drops off at higher output powers. This power-dependent efficiency is most likely a result of dielectric losses in the discrete capacitor elements. This result indicates that a benefit of the radial stub design is higher power handling capability.

The radial combiner is further characterized in the outphasing system operating at full power (branch supplies at 28 V) as shown in Fig. 16. Under these conditions, the system has a peak CW efficiency of 70% and an efficiency of over 60% for a 6.5-dB range. The system PAE is estimated as shown in Fig. 17 by applying the measured gain of a single branch PA (Fig. 13) to the drain efficiency measurement. According to this method, the PAE remains above 50% over a 7.8-dB power range.

In order to demonstrate that the relatively narrowband radial combiner system will operate over the entire 60-MHz range of channels required for W-CDMA, we also repeat the system characterization at the different carrier frequencies in the band. In Fig. 18, the peak output power and drain efficiency at various power back-off levels are shown as a function of carrier frequency over a 2110–2170 MHz range. These measurements indicate that the system will operate effectively over the entire range, and furthermore that the radial stub design can be fabricated as indicated in Fig. 6 for operation over the entire desired frequency range. The measured variation in peak output power, particularly at the higher end of the frequency range, can be explained as a combination of the variation in output power of the branch amplifiers over that range and the increase in reactive loading associated with shifting the carrier frequency from 2.14 GHz. The branch amplifier output power (into 50 Ω) varies by nearly 10% over this frequency range, with peak output power maximum at 2.12 GHz and minimum at 2.17 GHz.

B. Comparison to Chireix CW Performance

A Chireix outphasing system was implemented as shown in Fig. 19 to serve as a basis for comparison for the new four-way outphasing technique. In order to enable a direct comparison, the combiner input impedance range, combiner PCB, and branch amplifiers were set up to operate as analagously to those in the four-way system as possible (i.e., at the same total power level and with the same PAs, drivers, and circuit technology); this is necessary to an accurate comparison of the capabilities of the two approaches. The Chireix combiner reactance values were chosen as in Fig. 1 ($X_1 = 35.6\ \Omega$, $X_2 = 48.78\ \Omega$, and $R_L = 50\ \Omega$) to match the operating range of the four-way combiner. Furthermore, as can be

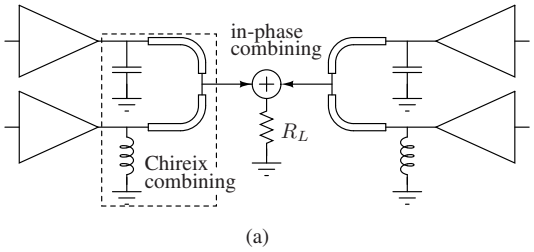

(a)

(b)

Fig. 19. Chireix system implementation, (a) – block diagram, and (b) – photograph. The combiner input impedance range, combiner PCB, and branch amplifiers were all selected for best comparison to the four-way outphasing system. The Chireix combiners were implemented in microstrip in the same technology as the four-way combiner. The in-phase combiner is realized with a very low-loss commercial combiner (RF HAMDESIGN 2320).

seen in Fig. 19, the combiner layout mimics that of the hybrid microstrip/discrete four-way combiner from Fig. 5 and similarly uses shunt discrete $C-C$ and $L-C$ components to synthesize the shunt reactances. This structure was fabricated on a 0.762-mm thick Rogers RO4350 substrate (as with the four-way combiner). The drain supply voltage of the branch amplifiers was 20 V to match the operating conditions of the hybrid microstrip/discrete four-way combiner. Lastly, in order to match the output power level of this demonstration to that of the four-way system for an even comparison, we in-phase combine the outputs of four branch PAs, operating in two Chireix systems, using a rat-race coupler chosen for its high power rating and very low insertion loss (RF HAMDESIGN 2320). With this final power combining stage included, the Chireix-based system can be most directly compared to the four-way system in terms of efficiency at a given power level. Note that an alternative configuration in which the output of two pairs of branch PAs are in-phase combined with their outputs combined in a Chireix outphasing system would also enable direct comparison. In that configuration, there would be further losses in the Chireix combiner associated with high power levels (as appeared in the comparison of hybrid microstrip/discrete and radial-stub four-way combiners in Section V-A), making the comparison less favorable to the Chireix combiner. Furthermore, the configuration used here was chosen as it results in the most similar branch PA loading conditions between the two combining approaches, including identical electrical lengths between the combiner and branch PA reference planes.

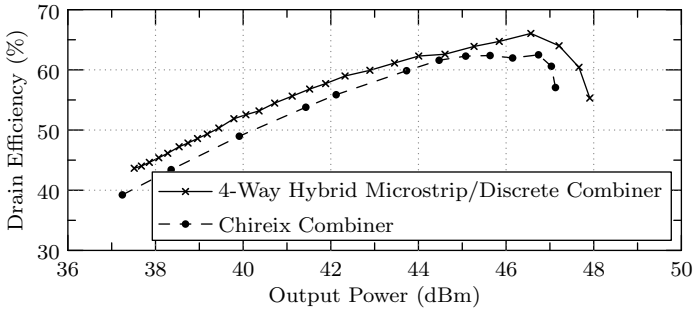

Fig. 20. CW performance comparison between the hybrid microstrip/discrete four-way combiner and Chireix outphasing systems. The combiners are constructed similarly and branch PAs in both systems are operated with 20-V drain supplies to accomodate the lower power-handling capability of the combiner incorporating discrete shunt elements. The four-way combiner provides an efficiency advantage of approximately 5% at most power levels, and enables a maximum output power that is approximately 0.8 dB (20%) higher than with the Chireix-based system.

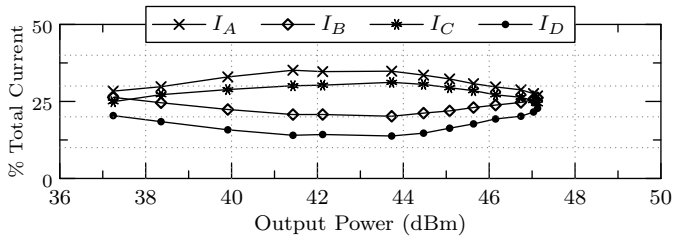

(a)

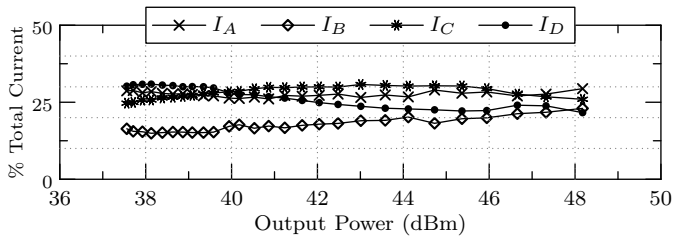

(b)

Fig. 21. Drain current distribution among the four branch PAs in the (a) – Chireix system, and (b) – four-way outphasing system. Accounting for variation in PA performance (see Fig. 12) these current distributions follow the expected PA loading in each system, with the 4-way combining providing more even loading of the PAs.

The CW measurements of the Chireix system are shown in Fig. 20. As for the four-way outphasing system measurements, the control law used is based on a combination of outphasing and drive modulation, where the input drive power is chosen experimentally to maximize drain efficiency. The individual AM/AM and AM/PM behavior of the branch PAs is characterized and compensated for using a memoryless LUT. These measurements show that the 4-way system provides an efficiency benefit of approximately 5% at most power levels, and enables a maximum output power that is approximately 0.8 dB (20%) higher than with the Chireix system. This represents a substantial advantage of the 4-way combining system. The advantage of the four-way combining system is further highlighted in Fig. 21, which shows the distribution of drain currents in the four-way and Chireix outphasing systems. Accounting for variation in PA performance (particularly the

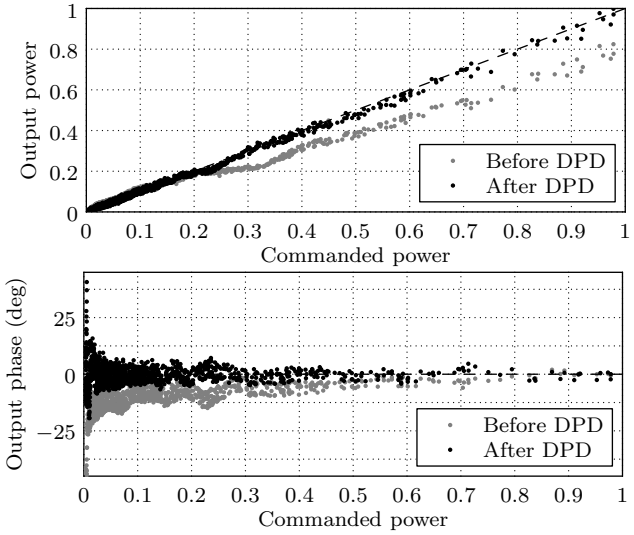

Fig. 22. Measured AM/AM and AM/PM distortion in the outphasing system with radial stub combiner before and after limited memoryless DPD is applied.

TABLE III
COMPARISON TO OTHER WORKS: W-CDMA PERFORMANCE

Ref.	Arch	Carrier (MHz)	CW P_{max} (W)	PAPR (dB)	$ACLR_1$ (dBc)	Drain Eff.
[38]	Chireix	2300	70	9.6	-49	53.5%
[47]	Chireix	2140	90	9.6	-47	50.5%
[37]	Chireix	1950	19	7.5	-47	65.1%
				9.6	-47	54.5%
[6]	4-way Doherty	2140	100	6.5	-31*	61%
[48]	Saturated Doherty	2140	10	7.4	28.3*	52.4%
[16]	4-way Discrete	2140	50	3.5	-36.6	57%
This Work	4-way Hybrid	2140	62	9.11	-31.9	50.3%
	4-way Radial	2140	110	9.15	-33.0	55.6%

* no predistortion

branch B PA in the four-way system which corresponds to PA:1 in Fig. 12) these current distributions follow the expected PA loading in each system, with the 4-way combining providing more even loading of the PAs.

C. Modulated Performance

The results of modulated testing with a 3.84-MHz, 9.15-dB PAPR W-CDMA signal are summarized in Table III. The radial stub combiner operates with 55.6% drain efficiency and 14.1 W average output power. With the limited DPD described in Section IV, the measured ACLR is -33.0 dBc. The improvement in linearity due to this memory-less DPD is shown in Fig. 22 in terms of AM/AM and AM/PM distortion. The hybrid microstrip/discrete combiner, with branch PA supplies set at 20 V because of the combiner's power limitations, operates with 50.5% average efficiency and 7.2 W average power, with -31.9 dBc ACLR and 9.11 dB measured PAPR. Compared to the hybrid microstrip/discrete combining network, the radial stub combiner therefore achieves 2.92-dB higher average modulated power and 5.3% higher average efficiency. The apparent advantage of both of these techniques over the very first microwave demonstration of this four-way power combining technique [16] (also indicated in Table III) is due to a combination of reduced combining network losses and improvements in the branch amplifier performance. Direct comparisons to other works are complicated by differing PAPRs and power levels, but it is clear that this first-generation system has performance on par with other high-performance architectures and implementations. It is also clear that further refinement (such as integration of the system to remove connector losses and more sophisticated digital predistortion) will enable still higher performance with this new technique.

VI. CONCLUSION

Outphasing amplifiers are increasingly attractive solutions for linear and efficient amplification in communications applications. In this work we investigate an outphasing architecture that provides nearly ideal resistive load modulation to the branch amplifiers. Whereas conventional outphasing techniques exhibit sub-optimal loading conditions, the one presented in this work has a high power factor even over a 60-MHz frequency range at 2.14 GHz. In the limit of switched-mode branch amplifiers, the four-way outphasing and combining system can in principle approach lossless operation.

In order to enable microwave operation of this technique, we have introduced two implementations of the four-way power combining network that are suitable for microwave applications. On one hand, we demonstrate a implementation of the four-way outphasing and combining system that enables tuning of component values, while including microstrip interconnects and discrete components in a manner that make this design appropriate for microwave frequencies. This implementation is compared to a Chireix-based outphasing system designed to match the operating conditions of the four-way system as closely as possible for an even comparison. In CW measurements, the hybrid microstrip/discrete four-way combiner provides an efficiency advantage of approximately 5% at most power levels, and enables a maximum output power that is approximately 0.8 dB (20%) higher than with the Chireix-based system, along with more even loading of the PAs as indicated by the distribution of drain currents among the four branch amplifiers. The alternative all-microstrip radial-stub-based combiner achieves greater repeatability and manufacturability by eliminating the need for hand-tuning of reactive elements, but has reduced bandwidth. Nonetheless, CW measurements of this system made over a 60-MHz range around 2.14 GHz indicate that the amplifier is able to operate over the entire W-CDMA frequency range. When compared at the same power level to the hybrid microstrip/discrete implementation, the radial-stub-based design is seen to have higher efficiency at the upper range of output powers. The four-way radial stub power combining network is also operated at higher power levels and has been demonstrated at up to 110 W peak CW

power. In CW outphasing measurements, the system has a peak drain efficiency of 70%, and drain efficiency over 60% for a 6.5-dB output power range. To demonstrate the efficiency performance of this new all-microstrip design, the system was driven with a 3.84 MHz W-CDMA signal with a 9.15-dB PAPR. The average modulated efficiency was 55.6% at an average power of 14.1 W. The performance of this first connectorized implementation is on par with the state of the art W-CDMA amplifiers using similarly advanced architectures and at similar power levels, and it is expected that refinement (such as integration of the PAs with the combiner) will enable significant further improvements. It is anticipated that with continued development this architecture will find widespread use in RF power amplification.

APPENDIX

COMPONENT TUNING PROCESS FOR HYBRID MICROSTRIP/DISCRETE COMBINER

The discrete component values for the hybrid microstrip/discrete combining network of Figs. 3, 5 are selected through an iterative tuning process in order to address the non-idealities of the components. As in [16], [43], the network is driven as a power splitter, i.e. by driving the output port, and the forward voltage gains to the four 50-Ω-terminated input ports are measured. In order to isolate the effects of mismatch in the $\pm jX_1$ and $\pm jX_2$ branches, the $\pm jX_2$ components are populated while the $\pm jX_1$ components are omitted so that there is (ideally) an even power split between the A and B (and C and D) branches. Components C_7, C_8, C_9, and L_3 (see Fig. 5) are then adjusted until the magnitude of the forward voltage gain from the output to ports A and C (or B and D) are equal and the phases have the expected relationship. Once the values for $\pm jX_2$ are established, the process is repeated to set the relationships between ports A and B, and between C and D by populating the $\pm jX_1$ components. The appropriate adjustment can be derived for each possible combination of mismatch in amplitude and phase from an analysis of the network. For example, if the voltage gain to port A is found to be higher than to port C, and the phase difference between the two ports is higher in magnitude than expected, the reactance corresponding to a nominal $+jX_2$ must be too small and C_9 is increased accordingly. The complete tuning strategy is summarized in Table IV. Although shown for the $\pm jX_2$ components, this approach can be directly applied to the $\pm jX_1$ match as well. Note that one typically fixes the inductors and only tunes capacitors (e.g., using values ranging from 0.1 pF to 2.7 pF), as a result of the limited number of available inductor values.

TABLE IV
COMPONENT TUNING STRATEGY BASED ON OBSERVING THE RELATIVE MAGNITUDES AND PHASES AT THE COMBINER INPUT PORTS WHEN THE NETWORK IS DRIVEN AS A SPLITTER.

Measured port relationship		Correction
$\frac{\lvert A\rvert}{\lvert C\rvert} > 1$	$\lvert\angle AC\rvert >$ ideal	C_9 $\uparrow$
	$\lvert\angle AC\rvert <$ ideal	C_7, C_8 $\uparrow$
$\frac{\lvert A\rvert}{\lvert C\rvert} < 1$	$\lvert\angle AC\rvert >$ ideal	C_7, C_8 $\downarrow$
	$\lvert\angle AC\rvert <$ ideal	C_9 $\downarrow$

Note: this method can be directly translated to component tuning for the $\pm jX_1$ branches by substituting branch B for C (or branches C and D for A and C) and correcting the appropriate capacitors in those branches.

REFERENCES

[1] F. Raab, P. Asbeck, S. Cripps, P. Kenington, Z. Popovic, N. Pothecary, J. Sevic, and N. Sokal, "Power amplifiers and transmitters for RF and microwave," *IEEE Trans. Microw. Theory Tech.*, vol. 50, no. 3, pp. 814 –826, Mar. 2002.

[2] J. Moon, J. Lee, R. Pengelly, R. Baker, and B. Kim, "Highly efficient saturated power amplifier," *IEEE Microwave Magazine*, vol. 13, no. 1, pp. 125–131, Jan.-Feb. 2012.

[3] M. Helaoui and F. Ghannouchi, "Optimizing losses in distributed multiharmonic matching networks applied to the design of an RF GaN power amplifier with higher than 80% power-added efficiency," *IEEE Trans. Microw. Theory Tech.*, vol. 57, no. 2, pp. 314–322, 2009.

[4] M. Roberg, J. Hoversten, and Z. Popovic, "GaN HEMT PA with over 84% power added efficiency," *Electronics Letters*, vol. 46, no. 23, pp. 1553 –1554, 11 2010.

[5] M. Pelk, W. Neo, J. Gajadharsing, R. Pengelly, and L. de Vreede, "A high-efficiency 100-W GaN three-way doherty amplifier for base-station applications," *IEEE Trans. Microw. Theory Tech.*, vol. 56, no. 7, pp. 1582–1591, 2008.

[6] A. Grebennikov, "A high-efficiency 100-W four-stage Doherty GaN HEMT power amplifier module for WCDMA systems," in *IEEE MTT-S Int. Microw. Symp. Dig.*, June 2011, pp. 1–4.

[7] H. Deguchi, N. Watanabe, A. Kawano, N. Yoshimura, N. Ui, and K. Ebihara, "A 2.6GHz band 537W peak power GaN HEMT asymmetric Doherty amplifier with 48% drain efficiency at 7dB," in *IEEE MTT-S Int. Microw. Symp. Dig.*, June 2012, pp. 1–3.

[8] D. Kimball, J. Jeong, C. Hsia, P. Draxler, S. Lanfranco, W. Nagy, K. Linthicum, L. Larson, and P. Asbeck, "High-efficiency envelope-tracking W-CDMA base-station amplifier using GaN HFETs," *IEEE Trans. Microw. Theory Tech.*, vol. 54, no. 11, pp. 3848–3856, 2006.

[9] H. Tango, T. Hashinaga, K. Totani, H. Kuriyama, Y. Hamada, and T. Asaina, "A 60% efficient envelope tracking power amplifier for 40W, 2.6GHz LTE base station with in/output harmonic tuning," in *IEEE MTT-S Int. Micro. Symp. Dig.*, June 2013, pp. 1–4.

[10] L. Kahn, "Single-sideband transmission by envelope elimination and restoration," *Proc. IRE*, vol. 40, no. 7, pp. 803 –806, July 1952.

[11] J. Hoversten, S. Schafer, M. Roberg, M. Norris, D. Maksimovic, and Z. Popovic, "Codesign of PA, supply, and signal processing for linear supply-modulated RF transmitters," *IEEE Trans. Microw. Theory Tech.*, vol. 60, no. 6, pp. 2010–2020, 2012.

[12] J. García, R. Marante, M. N. Ruiz, and G. Harnández, "A 1 GHz frequency-controlled class E^2 DC/DC converter for efficiently handling wideband signal envelopes," in *IEEE MTT-S Int. Microw. Symp. Dig.*, June 2013, pp. 1–4.

[13] F. Raab, "High-efficiency linear amplification by dynamic load modulation," in *IEEE MTT-S Int. Microw. Symp. Dig.*, June 2003, pp. 1717–1720.

[14] ——, "Electronically tuned power amplifier," US Patent 7,202,734, April 2007.

[15] H. Nemati, C. Fager, U. Gustavsson, R. Jos, and H. Zirath, "Design of varactor-based tunable matching networks for dynamic load modulation of high power amplifiers," *IEEE Trans. Microw. Theory Tech.*, vol. 57, no. 5, pp. 1110–1118, 2009.

[16] T. W. Barton, J. L. Dawson, and D. J. Perreault, "Experimental validation of a four-way outphasing combiner for microwave power amplification," *IEEE Microw. Wireless Compon. Lett.*, vol. 23, no. 1, pp. 28–30, Jan. 2013.

[17] T.-P. Hung, D. Choi, L. Larson, and P. Asbeck, "CMOS outphasing class-D amplifier with Chireix combiner," *IEEE Microw. Wireless Compon. Lett.*, vol. 17, no. 8, pp. 619–621, 2007.

[18] S. Lee and S. Nam, "A CMOS outphasing power amplifier with integrated single-ended Chireix combiner," *IEEE Trans. Circuits Syst. II: Exp. Briefs*, vol. 57, no. 6, pp. 411–415, 2010.

[19] F. Raab, "Efficiency of outphasing RF power-amplifier systems," *IEEE Trans. Commun.*, vol. 33, no. 10, pp. 1094–1099, Oct. 1985.

[20] A. Birafane and A. Kouki, "On the linearity and efficiency of outphasing microwave amplifiers," *IEEE Trans. Microw. Theory Tech.*, vol. 52, no. 7, pp. 1702–1708, July 2004.

[21] J. Yao and S. Long, "Power amplifier selection for LINC applications," *IEEE Trans. Circuits Syst. II: Exp. Briefs*, vol. 53, no. 8, pp. 763–767, Aug. 2006.

[22] F. Raab, P. Asbeck, S. Cripps, P. Kenington, Z. Popovic, N. Pothecary, J. Sevic, and N. Sokal, "RF and microwave power amplifier and transmitter technologies – part 3," *High Frequency Electronics*, pp. 34–48, Sept. 2003.

[23] R. Langridge, T. Thornton, P. Asbeck, and L. Larson, "A power reuse technique for improved efficiency of outphasing microwave power amplifiers," *IEEE Trans. Microw. Theory Tech.*, vol. 47, no. 8, pp. 1467–1470, Aug. 1999.

[24] X. Zhang, L. Larson, P. Asbeck, and R. Langridge, "Analysis of power recycling techniques for RF and microwave outphasing power amplifiers," *IEEE Trans. Circuits Syst. II: Analog Digit. Signal Process.*, vol. 49, no. 5, pp. 312–320, 2002.

[25] P. Godoy, D. Perreault, and J. Dawson, "Outphasing energy recovery amplifier with resistance compression for improved efficiency," *IEEE Trans. Microw. Theory Tech.*, vol. 57, no. 12, pp. 2895–2906, 2009.

[26] D. Cox, "Linear amplification with nonlinear components," *IEEE Trans. Commun.*, vol. COM-23, pp. 1942–1945, Dec. 1974.

[27] I. Hakala, D. Choi, L. Gharavi, N. Kajakine, J. Koskela, and R. Kaunisto, "A 2.14-GHz Chireix outphasing transmitter," *IEEE Trans. Microw. Theory Tech.*, vol. 53, no. 6, pp. 2129–2138, June 2005.

[28] D. Perreault, "A new power combining and outphasing modulation system for high-efficiency power amplification," *IEEE Trans. Circuits Syst. I: Reg. Papers*, vol. 58, no. 8, pp. 1713–1726, Feb. 2011.

[29] N. Singhal, H. Zhang, and S. Pamarti, "A zero-voltage-switching contour-based outphasing power amplifier," *IEEE Trans. Microw. Theory Tech.*, vol. 60, no. 6, pp. 1896–1906, June 2012.

[30] M. El-Asmar, A. Birafane, M. Helaoui, A. Kouki, and F. Ghannouchi, "Analytical design methodology of outphasing amplification systems using a new simplified Chireix combiner model," *IEEE Trans. Microw. Theory Tech.*, vol. 60, no. 6, pp. 1886–1895, 2012.

[31] P. Landin, J. Fritzin, W. Van Moer, M. Isaksson, and A. Alvandpour, "Modeling and digital predistortion of class-D outphasing RF power amplifiers," *IEEE Trans. Microw. Theory Tech*, vol. 60, no. 6, pp. 1907–1915, 2012.

[32] A. Jurkov and D. Perreault, "Design and control of lossless multi-way power combining and outphasing systems," in *Midwest Symp. Circuits Syst.*, Aug. 2011, pp. 1–4.

[33] A. Jurkov, L. Roslaniec, and D. J. Perreault, "Lossless multi-way power combining and outphasing for high-frequency resonant inverters," *IEEE Trans. Power Electron.*, (to appear).

[34] T. Ni and F. Liu, "A new impedance match method in serial Chireix combiner," in *Asia-Pacific Microw. Conf.*, 2008, pp. 1–4.

[35] W. Gerhard and R. Knoechel, "Improved design of outphasing power amplifier combiners," in *German Microw. Conf.*, 2009, pp. 1–4.

[36] R. Beltran, F. Raab, and A. Velazquez, "HF outphasing transmitter using class-E power amplifiers," in *IEEE MTT-S Int. Microw. Symp. Dig.*, June 2009, pp. 757–760.

[37] M. van der Heijden, M. Acar, J. Vromans, and D. Calvillo-Cortes, "A 19W high-efficiency wide-band CMOS-GaN class-E Chireix RF outphasing power amplifier," in *IEEE MTT-S Int. Microw. Symp. Dig.*, June 2011, pp. 1–4.

[38] D. Calvillo-Cortes, M. van der Heijden, and L. de Vreede, "A 70W package-integrated class-E Chireix outphasing RF power amplifier," in *IEEE MTT-S Int. Microw. Symp. Dig.*, June 2013, pp. 1–3.

[39] H. Chireix, "High power outphasing modulation," *Proceedings of the IRE*, vol. 23, no. 11, pp. 1370–1392, Nov. 1935.

[40] L. Roslaniec and D. Perreault, "Design of variable-resistance class E inverters for load modulation," in *IEEE Energy Conversion Congr. Expo.*, 2012, pp. 3226–3232.

[41] S. Kee, I. Aoki, A. Hajimiri, and D. Rutledge, "The class-E/F family of ZVS switching amplifiers," *IEEE Trans. Microw. Theory Tech.*, vol. 51, no. 6, pp. 1677–1690, June 2003.

[42] A. Jurkov, L. Roslaniec, and D. Perreault, "Lossless multi-way power combining and outphasing for high-frequency resonant inverters," in *2012 Int. Power Electronics and Motion Control Conf.*, June 2012, pp. 910–917.

[43] T. W. Barton, J. L. Dawson, and D. J. Perreault, "Four-way lossless outphasing and power combining with hybrid microstrip/discrete combiner for microwave power amplification," in *IEEE MTT-S Int. Microw. Symp. Dig.*, June 2013, pp. 1–4.

[44] G. Kompa, *Practical Microstrip Design and Applications*. Norwood, MA: Artech House, 2005.

[45] Y. Han, O. Leitermann, D. A. Jackson, J. M. Rivas, and D. J. Perreault, "Resistance compression networks for radio-frequency power conversion," *IEEE Trans. Power Electron.*, vol. 22, no. 1, pp. 41–53, Jan. 2007.

[46] A. K. Mustafa, S. Ahmed, and M. Faulkner, "Bandwidth limitation for the constant envelope components of an OFDM signal in a LINC architecture," *IEEE Trans. Circuits Syst. I: Reg. Papers* (Early Online Access).

[47] J. Qureshi, M. Pelk, M. Marchetti, W. Neo, J. Gajadharsing, M. van der Heijden, and L. de Vreede, "A 90-W peak power GaN outphasing amplifier with optimum input signal conditioning," *IEEE Trans. Microw. Theory Tech.*, vol. 57, no. 8, pp. 1925–1935, Aug. 2009.

[48] J. Kim, J. Moon, Y. Y. Woo, S. Hong, I. Kim, J. Kim, and B. Kim, "Analysis of a fully matched saturated Doherty amplifier with excellent efficiency," *IEEE Trans. Microw. Theory Tech.*, vol. 56, no. 2, pp. 328–338, 2008.

Taylor W. Barton (S'07, M'12) received the Sc.D degree from the Massachusetts Institute of Technology (Cambridge, MA) in 2012 for her research in energy-efficient power amplifiers for wireless communications. She also holds Sc.B, M.Eng., and E.E. degrees from MIT's department of Electrical Engineering and Computer Science. In 2007 she joined the MIT Microsystems Technology Laboratory where she has also been a Postdoctoral Associate since 2013. Before starting as a post-doc, she was a visiting lecturer at MIT lecturing solid state circuits. Her research interests include high-efficiency RF and analog circuit design, and classical control theory.

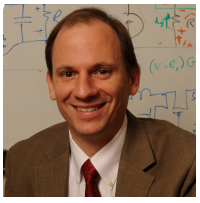

David J. Perreault (S91, M97, SM 06, F13) received the B.S. degree from Boston University, Boston, MA, and the S.M. and Ph.D. degrees from the Massachusetts Institute of Technology, Cambridge, MA. In 1997 he joined the MIT Laboratory for Electromagnetic and Electronic Systems as a Postdoctoral Associate, and became a Research Scientist in the laboratory in 1999. In 2001, he joined the MIT Department of Electrical Engineering and Computer Science, where he is presently Professor and Associate Department Head. His research interests include design, manufacturing, and control techniques for power electronic systems and components, and in their use in a wide range of applications. He also consults widely in industry, and is co-founder of Eta Devices, a startup company focusing on high-efficiency RF power amplifiers. Dr. Perreault received the Richard M. Bass Outstanding Young Power Electronics Engineer Award from the IEEE Power Electronics Society, an ONR Young Investigator Award, and the SAE Ralph R. Teetor Educational Award, and is co-author of six IEEE prize papers.